Hydrogen substitution of natural-gas in premixed burners and implications for blow-off and flashback limits

Andrea Aniello, Thierry Poinsot, Laurent Selle, Thierry Schuller

Hydrogen substitution of natural-gas in premixed burners and implications for blow-off and flashback limits

A. Aniello[a], T. Poinsot[a], L. Selle[a], T. Schuller[a]

[a] *Institut de Mécanique des Fluides de Toulouse, IMFT, Université de Toulouse, CNRS, France*

Abstract

Two multi-perforated premixed burners, designed for natural gas, are fuelled with increasing hydrogen content to assess the limits of H_2 substitution and investigate potential risks associated to it. The burners feature a different design, which affects flame stabilization and heat exchange between the fresh mixture and the hot burner walls. First, results are presented by means of stability maps that were collected at constant power and over a wide range of equivalence ratio, from pure methane-air to pure hydrogen-air mixtures. The impact of hydrogen addition on blow-off and flashback limits is then analyzed. On one side, it is observed that hydrogen addition increases blow off resistance, extending the operating range towards ultra-lean conditions. On the other side, hydrogen raises the thermal load on the burner favoring flashback. It is shown that the competition between the bulk velocity at the burner outlet and the laminar burning velocity is not a reliable parameter to predict flashback occurrence, while the thermal state of the burner represents a determining factor. An analysis of the thermal transient reveals a strict correspondence between the onset of flashback for a given mixture composition and the burner surface temperature. Results highlight the challenges linked to the design of fuel-flexible systems, pointing out practical limits of H_2 substitution in burners designed for operation with natural gas.

Keywords: HYDROGEN SUBSTITUTION, PREMIXED COMBUSTION, LEAN BLOW-OFF, FLASHBACK.
2020 MSC: 00-01, 99-00

1. Introduction

Hydrogen is a promising fuel to achieve decarbonization of combustion processes. It can be produced from renewable sources via electrolysis and distributed in the gas network upon request, following a Power-to-Gas pathway [1]. Hydrogen enhanced combustion is also considered in off-grid strategies

in which the local production is stored and later consumed as for example in isolated sites [2].
However, adding hydrogen to standard fuels poses challenges [3, 4], since it modifies fundamental combustion characteristics [5] that can compromise the fulfillment of safety and pollution standards. As result, burners designed for natural gas, can only sustain limited hydrogen concentrations, typically 5 to 20 $\%vol$ in the fuel blend (https://www.hydrogeneurope.eu, 29/01/2022). Even in the best scenarios, a hydrogen volume fraction of 20% would represent only 7% mass reduction of CO_2 per energy unit with respect to natural gas. In order to develop new burners able to accommodate higher hydrogen concentrations, there is a need for more fundamental studies to understand critical issues associated to its addition.

Commercial systems are not designed for research purposes and it is difficult to monitor and control separately basic variables to generalize results, such as thermal power P_{th} and equivalence ratio ϕ_{g}. Moreover, the variety of hardware and control systems adds further complexity to the evaluation of hydrogen effects. For example, several self-aspirating burners have been tested with increasing hydrogen content showing a variable H_2 tolerance with a burner temperature that was barely affected in one case and augmented by more than 60% in the other [6, 7, 8]. In self-aspirating burners the mixture composition depends on the air velocity at the fuel nozzle outlet, which creates a negative static pressure that sucks fuel into the oxidizer stream. As result, the equivalence ratio of the combustible mixture could not be controlled independently, so that the results are only valuable for the specific operating conditions tested.

Pioneering studies on unconfined laminar premixed Bunsen flames [9, 10, 11] demonstrated that the flame fronts stabilize where the flow velocity component perpendicular to the reaction front equals the laminar burning velocity, leading to a conical shaped flame. In particular, lowering the bulk velocity U_b in premixed system promotes flashbacks [12, 13], while higher values favor blow-off [9, 10]. These fundamental features have been studied since the early 1940s but, in spite of the empirical and numerical models proposed, they are not completely understood in practical configurations. Moreover, the flame structure is influenced by the local flow velocity, local flame curvature and thermodiffusive properties of the mixture [14, 15, 16, 17], which are particularly important for hydrogen [18, 19]. In addition, both measurements [20, 21, 22] and numerical simulations [23, 24] prove that heat losses towards the flame holder also affect flame stabilization and flame dynamics. A direct dependency between flame stand-off distance η, laminar burning velocity S_L, heat losses and flame temperature is demonstrated in [25, 26] for example. Heat recirculation has also been

shown to alter flame stabilization by preheating the incoming gases [25, 27, 28]. In order to explore the impact of all parameters, the gas mass flow rates, fuel composition and equivalence ratio must be controlled separately.

Several works performed on multi-perforated cylindrical burners, already outlined the effects of burner porosity σ and surface temperature T_w [29, 30]. Tests on the heat exchanger efficiency also demonstrated that the risk of flashback increases at lower thermal power [31], although experiments were not conducted at fixed equivalence ratio. Studies dedicated to full-scale burners highlighted that pollutant concentrations depend on the temperature distribution inside the combustion chamber [32]. The critical role of flame heat losses on NO_x production was analyzed in [33]. Recent studies revealed the impact of hydrogen enrichment in commercial devices in terms of flame stabilization and pollutant emissions [34, 35, 36, 37], but they do not consider flashback and blow off issues.

In the present work, the physical parameters that drive flame stabilization are identified and controlled, so that the impact of hydrogen addition on the operability of the systems is investigated. Two cylindrical premixed burners featuring different designs and used in condensing boilers are considered. The analysis is limited to forced draft burners, in which fresh gases are maintained above atmospheric pressure. Only the low power range is investigated, since low volumetric flow rates favor flashback and increase the thermal stress on the burner, which are two main concerns related to H_2 enrichment. First, the hydrogen and methane concentrations in the global mixtures are defined in Sec. 2. The description of the two burners and of the methodologies used to analyze the effect of hydrogen enrichment are provided in Sec. 3. The burners response to dual fuel methane-hydrogen mixtures is illustrated in Sec. 4 for two different powers via stability maps collected in steady state conditions. The effects of H_2 on blow-off and burner surface temperature is evaluated in Secs. 5 and 6, respectively. Finally, section 7 focuses on flashback limits.

2. Definition of hydrogen enriched admixtures

In this work, methane is used as a surrogate for natural gas. Methane and hydrogen are perfectly premixed before injection and the fresh gases are defined by the equivalence ratio ϕ_g and by the molar fraction of hydrogen X_{H_2} in the fuel blend. Considering the global balance equation for lean

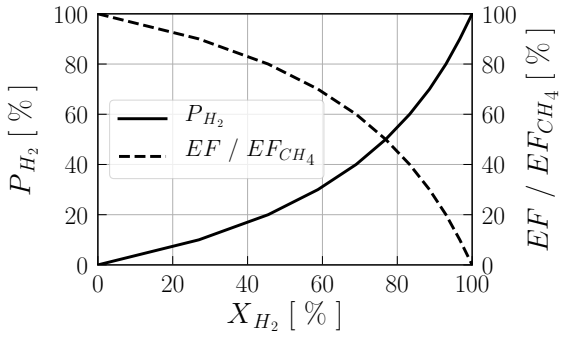

Figure 1: The solid line (———) illustrates the relation between the percentage of the total thermal power P_{th} provided by hydrogen oxidation $P_{\mathrm{H_2}}$ and the molar fraction of hydrogen $X_{\mathrm{H_2}}$ in the fuel blend. The dashed line (- - - -) shows the reduction percentage of the emission factor EF ($kg_{\mathrm{CO_2}}/J$) of hydrogen enriched mixtures with respect to pure methane combustion.

combustion of this multi-component fuel:

$$\phi_g(X_{\mathrm{CH_4}}\mathrm{CH_4} + X_{\mathrm{H_2}}\mathrm{H_2}) + (2 - \frac{3}{2}X_{\mathrm{H_2}})(\mathrm{O_2} + a\mathrm{N_2}) \rightarrow$$
$$\rightarrow \phi_g(X_{\mathrm{CH_4}}\mathrm{CO_2} + (2 - X_{\mathrm{H_2}})\mathrm{H_2O}) + (2 - \frac{3}{2}X_{\mathrm{H_2}})((1 - \phi_g)\mathrm{O_2} + a\mathrm{N_2}) \quad (1)$$

The global equivalence ratio ϕ_{g} is defined as α/α_s in which α is the ratio between the actual mass flow rates of fuel and air, while α_s represents its value at stoichiometry:

$$\alpha_s = \frac{X_{\mathrm{CH_4}}W_{\mathrm{CH_4}} + X_{\mathrm{H_2}}W_{\mathrm{H_2}}}{(2 - \frac{3}{2}X_{\mathrm{H_2}})(W_{\mathrm{O_2}} + aW_{\mathrm{N_2}})} \quad (2)$$

in which $a = 3.76$ and W_{k} is the molar weight of species k. The molar fraction of $\mathrm{H_2}$ in the fuel mixture is given by:

$$X_{\mathrm{H_2}} = \frac{\dot{n}_{\mathrm{H_2}}}{\dot{n}_{\mathrm{H_2}} + \dot{n}_{\mathrm{CH_4}}} \quad (3)$$

where $\dot{n}_{\mathrm{H_2}}$ and $\dot{n}_{\mathrm{CH_4}}$ are the molar flow rates of hydrogen and methane. Since the fuel is a binary mixture, the methane molar fraction corresponds to $X_{\mathrm{CH_4}} = 1 - X_{\mathrm{H_2}}$.

It is also useful to define the amount of hydrogen in the fuel considering the percentage of the total thermal power P_{th} provided by hydrogen oxidation:

$$P_{\mathrm{H_2}} = \frac{X_{\mathrm{H_2}}Q_{\mathrm{H_2}}}{X_{\mathrm{CH_4}}Q_{\mathrm{CH_4}} + X_{\mathrm{H_2}}Q_{\mathrm{H_2}}} \quad (4)$$

where Q_{H2} and Q_{CH4} are the molar lower heating values of hydrogen and methane. On one hand, this definition allows to compare operating conditions at constant power, which is a critical

design parameter. On the other hand, P_{H_2} is equal to the reduction in CO_2 emission associated to hybridization. The nonlinear relations between P_{H_2} and X_{H_2}, as well as the reduction percentage in CO_2 mass emission per energy unit caused by hydrogen enrichment EF / EF_{CO_2}, are plotted in Fig. 1.

3. Materials and methods

3.1. Experimental setup

Air and CH_4 and H_2 mix directly into the supply lines, ensuring the injection of a fully premixed charge at the bottom of the bench displayed in Fig. 2. Mass flow rates are individually controlled using three mass flow meters and regulators: Vögtlin instruments GSC-B for air and H_2, Bronkhorst F-201CV for CH_4. This allows to control independently the hydrogen substitution in the fuel P_{H_2}, the equivalence ratio ϕ_g and the total thermal power P_{th} over a wide range of operating conditions. Once injected, the mixture is guided via a diverging duct into a cylindrical plenum with a diameter of 90 mm. It passes through a SiC porous structure characterized by 80% porosity and 40 mm thickness which breaks down the large flow structures and acts like a flame arrestor in case of flashback. For safety, a K-type thermocouple is also installed inside the plenum to measure the incoming gas temperature. Finally, the laminar flow feeds the cylindrical burner as shown in Fig. 2. The burner is tested without the confinement of the combustion chamber and heat exchanger, which are instead part of the commercial system. This open configuration ensures optical access to the combustion region, but it may lead to results that deviate quantitatively from practical operations.

3.2. Wall and gas temperature measurements

A two-color infrared pyrometer (FLUKE Endurance series) with spectral response between 1.5 μm and 1.6 μm is used to measure the surface temperature T_w of the burner to avoid overheating and verify convergence towards steady state condition. With the double wavelength approach the temperature measurements can be performed irrespective of the surface emissivity, which depends on material surface properties and temperature. The pyrometer operates between 250°C and 1200°C, with a precision of ± 0.3%.

In order to account for the preheating of the fresh gases by the hot burner wall, flow temperature measurements in front of the small burner holes are performed following the technique presented in [27]: the burner operates in steady state condition when the fuel rate is shut forcing flame

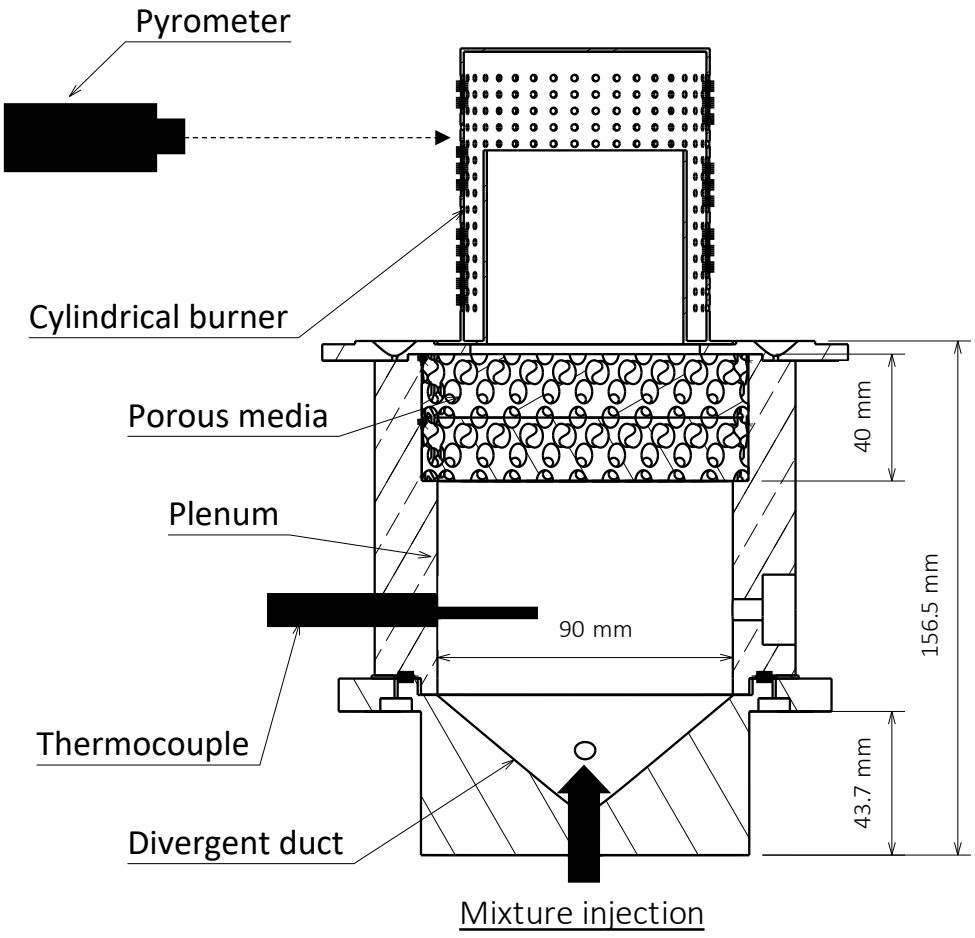

Figure 2: Schematic representation of the test bench cross sectional area with on board instrumentation.

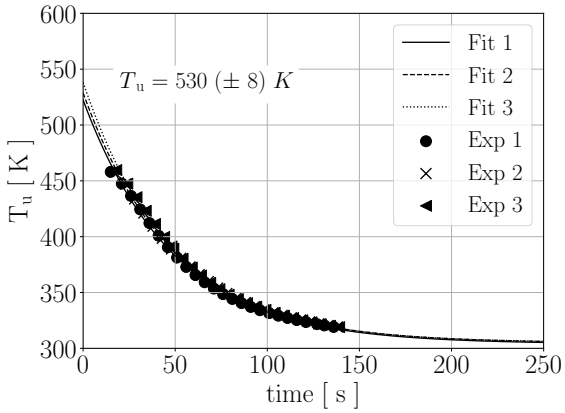

Figure 3: Example of the exponential fitting for experimental data to evaluate the fresh gas preheating due to the burner hot walls. Three independent gas temperature measurements over time are shown using the burner $B1$ at 4 kW for P_{H_2}= 40 % and $\phi_g = 0.6$.

quenching; this instant corresponds to the initial time of data acquisition and a movable K-type thermocouple is placed near the external multi-perforated surface of the burner to measure the gas flow temperature exhausting the burner; after a certain time delay, related to the thermal inertia of the thermocouple itself, temperature decreases exponentially following the gas temperature reduction and data are collected with 5 seconds interval; finally an extrapolation between the time corresponding to the first valid signal acquisition and initial instant $t = 0$ is performed to retrieve the preheating temperature of the gas at the instant preceding quenching. Figure 3 shows the result of the extrapolation obtained from three independent gas temperature T_u measurements performed with the burner $B1$ at 4 kW for P_{H_2}= 40 % and $\phi_g = 0.6$. It shows that the method yields repeatable results with a uncertainty of about ± 10 K.

3.3. Velocity measurements

A hot wire (MiniCTA - Dantec Dynamics) is used to determine the velocity component in the radial direction, perpendicular to the burner holes. The probe is positioned at a distance $d = 0.5$ mm from the burner wall, while the hot wire is moved along the burner longitudinal direction (see Fig. 10(b)). Velocity measurements are taken with a spatial resolution of 0.1 mm, ensuring at least 4 points inside the diameter of a single burner hole. Each value is the average of measurements performed with a sampling frequency of 1 Hz over a duration of 5 seconds.

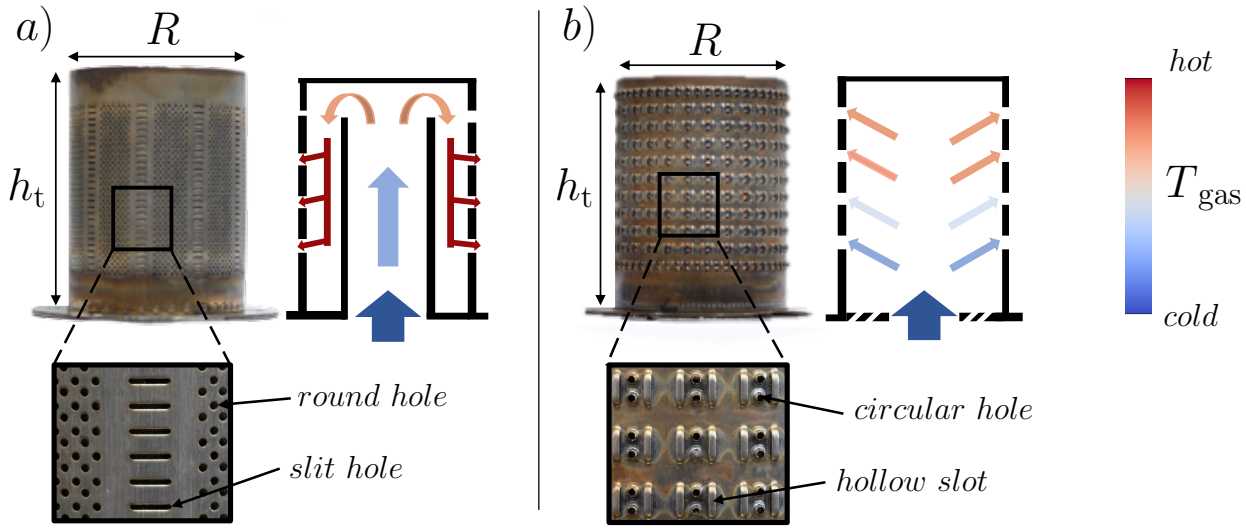

Figure 4: Illustration of external and internal designs of the burners $B1$ (a) and $B2$ (b) with qualitative description of the evolution of the gas stream temperature inside the burners. The two zoom-boxes at the bottom of each image represent a detailed view of the exit hole pattern for each burner.

	h_t (mm)	R (mm)	σ (%)
$B1$	95.0	70.4	8
$B2$	92.0	69.7	3

Table 1: Dimensions and external surface porosity values of burners B1 and B2 shown in Fig. 4.

3.4. Burners description

The forced draft burners $B1$ and $B2$ are representative of two technologies used in residential condensing boilers and designed to operate between 2 and 30 kW with natural gas.

Figures 4(a-b) display photos of the two burners with a sketch of their internal structure. They are made of stainless steel and feature similar sizes (Tab. 1). Burner $B1$ is characterized by both round and slit holes (Fig. 4(a)). Circular holes have 0.5 mm diameter with $l = 2.5$ mm pitch and the slits are 4.0 mm wide by 0.5 mm long. Burner $B1$ features a double metallic layer with a small gap that makes a U-turn to guide the flow through the holes. For the burner $B2$ (Fig. 4(b)), the outlets are distributed following the repetition of the same geometrical pattern: two circular holes of 0.7 mm

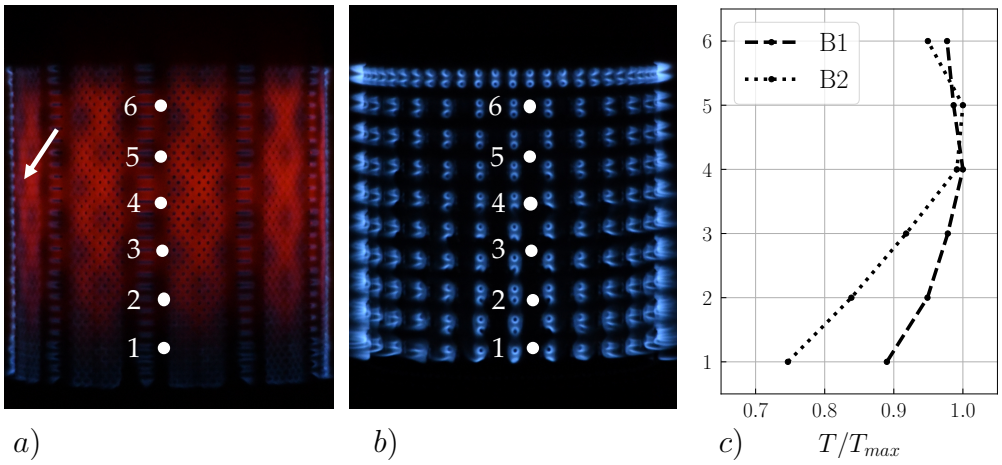

Figure 5: Qualitative view of the burner surface temperature at steady state conditions for burners $B1$ and $B2$ at the same operating condition: $\phi_g = 0.60$, $P_{H_2} = 40\%$ and 4 kW. Burner $B1$ (a) exhibits higher surface temperatures and higher thermal radiation than $B2$. The mean normalized wall temperature distribution from locations 1 to 6 along the axial direction is shown in (c). The white arrow put in evidence the small flames anchored at the burner wall.

diameter and two lateral hollow slots. This pattern is reproduced periodically along the burner tangential and axial directions with a step of 6.7 mm and 7.2 mm, respectively. Since the apertures of the hollow slots point towards the circular holes, the structure of the flow at the flame base is more complex for the burner $B2$ than burner $B1$. Also, a swirler is used at the inlet of the burner that helps to homogenize the flow at the burner hole outlets. Over the conditions investigated the pressure losses characterizing the two burners are comparable and limited between 20 Pa and 50 Pa.

These two designs result in different burner porosities $\sigma_{B_1} = 8\%$ and $\sigma_{B_2} = 3\%$ which, considering constant volumetric flow rate and gas inlet temperature, leads to a strong difference in bulk flow velocities $U_b^{B_1}$ and $U_b^{B_2}$ through the holes:

$$U_b^{B_2} = \frac{\sigma_{B_1}}{\sigma_{B_2}} U_b^{B_1} \simeq 2.7 U_b^{B1} \tag{5}$$

This definition of the bulk flow velocity does not account for the non-uniformity of the flow field along the burner or for the specific geometry of the outlets and must be considered as an average value.

Figure 5(a-b) displays direct views of flames in both burners at $\phi_g = 0.6$ and $P_{H_2} = 40\%$ showing

$B1$		$B2$	
ϕ_{g} - $P_{\mathrm{H_2}}$	T_{max} [K]	ϕ_{g} - $P_{\mathrm{H_2}}$	T_{max} [K]
0.6 - 40%	635	0.6 - 70%	658
0.7 - 20%	698	0.7 - 50%	695
0.8 - 0%	718	0.8 - 30%	714

Table 2: List of operating conditions at 4 kW used to provide the average normalized axial wall temperature profile for burners $B1$ and $B2$ in Fig. 5(c).

that the surface of burner $B1$ produces a stronger thermal radiation than $B2$, since flames stabilize closer to the metallic surface of $B1$ leading to higher temperatures of the burner walls. Figure 5(c) shows the mean normalized temperature distribution along the vertical direction for both burners. Temperature profiles were normalized by the maximum wall temperature T_{w} for each operating conditions synthesized in Tab. 2 and then averaged separately for burner $B1$ and $B2$. For each burner, the normalised temperature distribution remains roughly the same for all conditions explored. Measurements taken at locations 1 to 6 as indicated in Fig. 5(a-b) also show that the temperature is more uniform along burner B1. For both burners the highest temperature occurs between locations 4 and 5. At the top and at the bottom of the burner, the wall temperature decreases due to heat losses. The relative temperature reduction at the bottom of burner $B2$ is much stronger than in burner $B1$. Moreover, the internal structure itself also influences the gas residence time inside the burner, affecting the temperature T_u at which the unburned gases exit the burner holes. As sketched in Fig. 4, burner $B1$ favors preheating, since the fresh mixture makes a U-turn at the top of the burner resulting in a longer residence time of the reactants. Inside $B2$, instead, the mixture is directly distributed over the external surface limiting the heat transfer to the flow. This effect is illustrated in Tab. 3. The preheating temperature of the fresh gases is measured at given wall temperature T_{w} for burners $B1$ (T_u^{B1}) and $B2$ (T_u^{B2}). The wall temperature T_{w} is adjusted tuning the hydrogen content $P_{\mathrm{H_2}}$ at constant equivalence ratio, minimizing the variation on the total mass flow rate. Table 3 shows that burner $B1$ promotes larger heat transfer to the reactants than burner $B2$. The same wall temperature results in greater preheating of the reactants with burner $B1$. In the rest of the study, T_{w} must be considered as the wall temperature measured at location 4 in Figs. 5(a-b).

$\phi_{\mathbf{g}}$	PH_2^{B1}	PH_2^{B2}	$T_{\mathbf{w}}$ (K)	T_u^{B1} (K)	T_u^{B2} (K)
0.6	16%	48%	750 ± 2.3	531 ± 5	466 ± 11
0.6	28%	67%	850 ± 2.6	568 ± 22	475 ± 16
0.7	15%	50%	950 ± 2.9	652 ± 13	555 ± 10

Table 3: Preheated gas temperatures T_{u} for burners $B1$ and $B2$ are compared at fixed wall temperature T_{w}. The burners are operated at the same equivalence ratio to minimize the mass flow variations. The hydrogen content is tuned to match the targeted wall temperature T_{w} with the different burners.

4. H_2 hybridization impact on stabilization maps

Figures 6(a-d) present burners stability maps performed at constant power of 2 kW (at the bottom) and 4 kW (at the top) for burner $B1$ (left) and burner $B2$ (right) as a function of the hydrogen enrichment $P_{\mathrm{H_2}}$ and global equivalence ratio ϕ_{g}. At constant hydrogen content $P_{\mathrm{H_2}}$ the equivalence ratio ϕ_{g} is changed by modulating the air mass flow rate and, due to limitations of the air mass flow controllers, its minimum value is $\phi_{\mathrm{g}} = 0.45$ at 4 kW and $\phi_{\mathrm{g}} = 0.30$ at 2 kW. Three isolines representative of the ratio $U_b/S_l = 1$, calculated for mixture temperatures $T_{\mathrm{u}} = 300$ K (red), 500 K (green) and 700 K (blue), are superposed on the maps and will be discussed in Sec. 7. The maps illustrate the combinations of $P_{\mathrm{H_2}}$ and ϕ_{g} that allow to operate the burners without facing undesirable events, namely blow-off, overheating and flashback:

- Blow-off is defined here as the condition at which the flames detach from the lower side of the burner, leading to incomplete combustion.
- Overheating occurs when the burner surface temperature T_{w} overcomes 1050 K, which is the one measured for $B1$ at the reference condition of $P_{\mathrm{H_2}} = 0\%$, $\phi_{\mathrm{g}} = 0.8$ and $P_{\mathrm{th}} = 4$ kW.
- Flashback happens when the flame front propagates upstream through the injection system [38].

Figures 6(a-d) show that stable operating conditions, regardless of the burner and the power investigated, are limited by two main boundaries: one at the bottom-left side of the maps and the other at the top-right side. The first corresponds to the blow-off (----). For a given hydrogen content $P_{\mathrm{H_2}}$, the reduction of the equivalence ratio ϕ_{g} decreases the reactivity of the mixture and the flames blow-out. Interestingly, increasing the hydrogen content $P_{\mathrm{H_2}}$ the blow-off limit occurs at lower equivalence ratios and it is possible to sustain leaner combustion for both burners. For

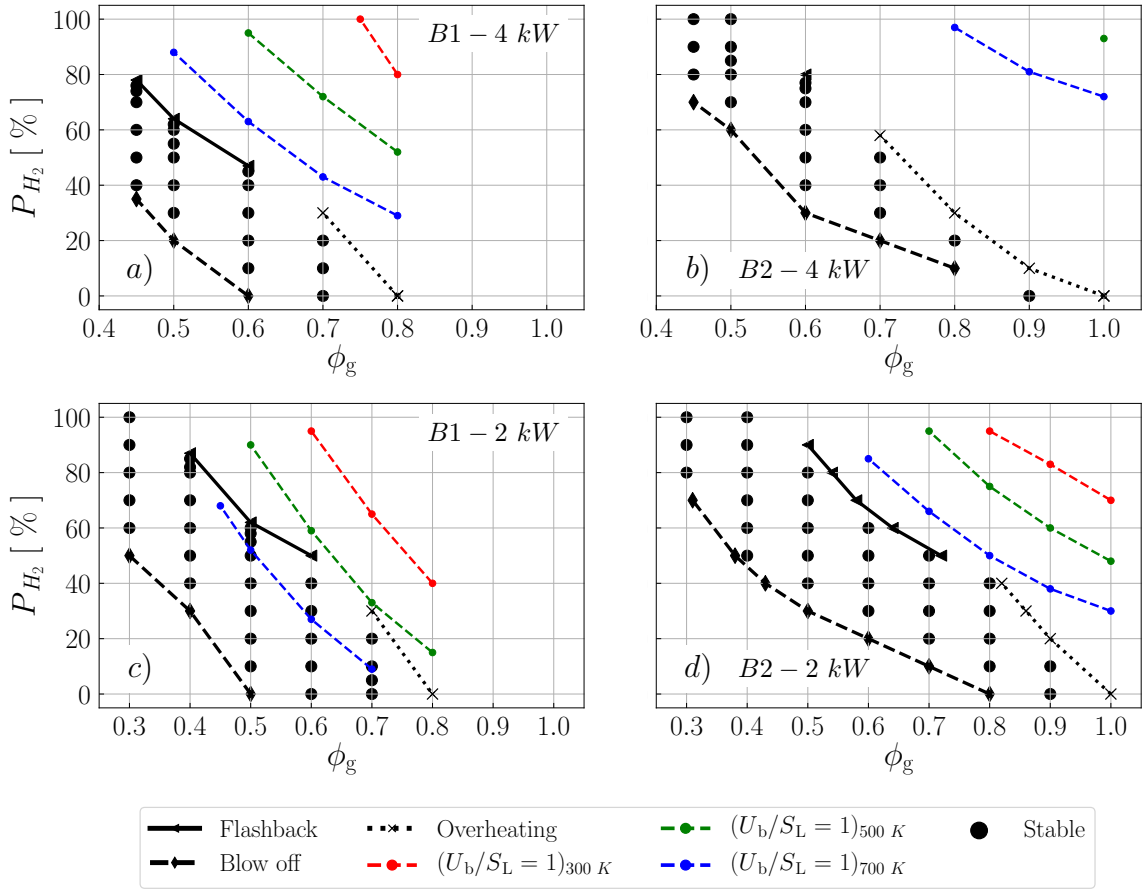

Figure 6: Steady-state stabilization maps displaying stable operating conditions as function of equivalence ratio ϕ_g and H_2 content P_{H_2}. Plots refer to burner $B1$ operated at 4 kW (a) and 2 kW (c) and to burner $B2$ operated at 4 kW (b) and 2 kW (d), showing the operating limits associated to blow-off (- - - -), flashback (———) overheating (·····). The red, green and blue curves on each plot identify the isolines at $U_b/S_L = 1$ for fresh gas temperature of T_u =300 K, 500 K and 700 K respectively.

instance, Fig. 6(a) shows that, increasing P_{H_2} from 0% to 40%, it is possible to reduce ϕ_g from 0.60 to 0.45. The other limits are overheating (·····) and flashback (——). Figures 6(a-d) indicate that the highest achievable hydrogen enrichment P_{H_2} is reduced by increasing the equivalence ratio ϕ_g, independently of the burner and thermal power. Closer to stoichiometry, the limiting factor is the thermal resistance of the material because, thanks to the greater reactivity of the mixture, flames stabilize closer to the burner surface promoting heat transfer to the wall. At leaner conditions, instead, the maximum hydrogen enrichment P_{H_2} is dictated by flashback, which occurs for burner surface temperatures below 1050 K. Nevertheless, Figs. 6(a-d) show that H_2 addition does not widen the range of achievable operating conditions: an improvement of the lean blow-off limit is systematically accompanied by a reduction of the highest achievable equivalence ratio due to overheating or flashback.

The aforementioned conclusions apply qualitatively to both burners. However, from a quantitative standpoint, differences are found between burners $B1$ and $B2$ for a constant power. On one hand, $B2$ exhibits a greater flashback resistance, allowing for higher hydrogen content at the same equivalence ratio. For example, at $P_{th} = 4$ kW and $\phi_g = 0.6$, flashback appears at $P_{H_2} = 50\%$ and $P_{H_2} = 80\%$ for $B1$ and $B2$, respectively. On the other hand, $B2$ is more prone to blow-off and a series of low-ϕ_g low-P_{H_2} operating conditions are only achievable with $B1$, as for example $P_{H_2} = 0\%$ and $\phi_g = 0.6$. To sum up, there are operating conditions that are stable for one burner and not achievable with the other, independently of power. Since the range of operating conditions is the same for both burners, these differences must be related to their design. Burner $B2$ generates higher bulk flow velocities U_b at the hole outlets and features a lower influence on the unburned gas temperature T_u than burner $B1$ (Sec. 3.4). As a matter of fact these aspects facilitate flame detachment from the wall, hindering flashback and eventually favoring blow-off. Thus, the hole pattern of the multi-perforated surface influences the performances of the burner. However, improving flashback tolerance worsens the blow-off resistance, limiting the effective fuel flexibility at fixed equivalence ratio.

5. Blow-off limit description

Hydrogen addition is known for improving the blow-off resistance [39, 40]. In this section, flame images are used to investigate the differences in the mechanisms leading to blow-off for different fuel blends in both burners. Images are taken with a NIKON D7500 camera, equipped with Micro-Nikkor 105 mm, from a direction tangent to the cylindrical surface of the burner (see Fig. 4(a)).

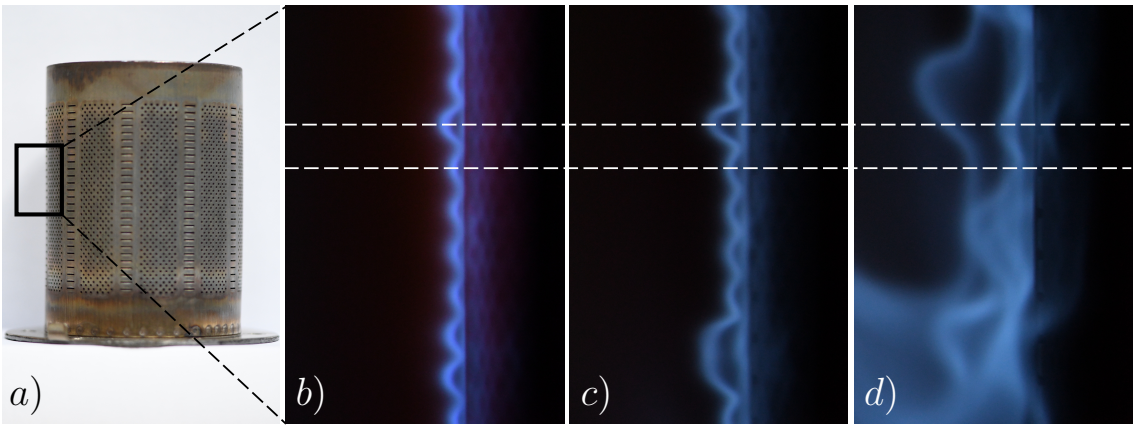

Figure 7: Flame shape along burner $B1$ longitudinal side, captured from a direction tangential to the burner surface above the slit holes as shown in (a). Operation at 4 kW with pure methane flames $P_{H_2} = 0\%$ at equivalence ratios (b) 0.70, (c) 0.65 and (d) 0.55.

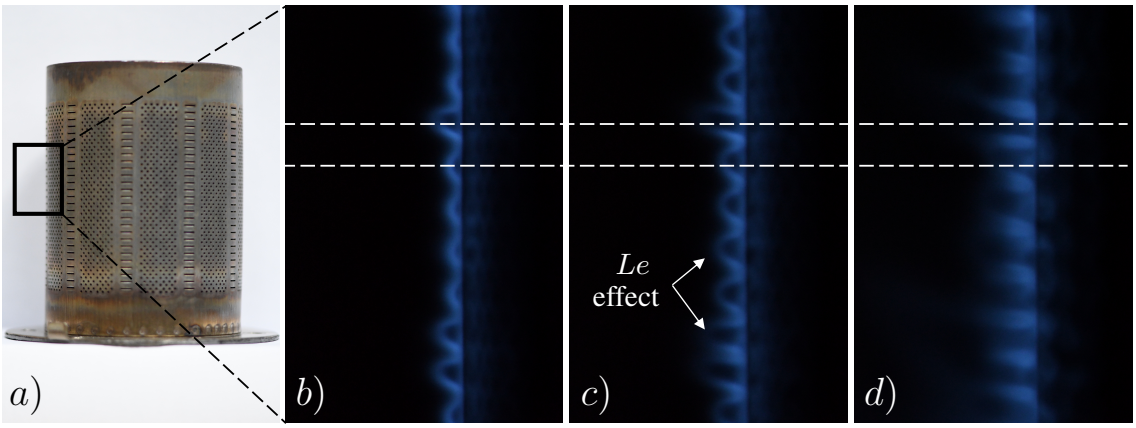

Figure 8: Flame shape along burner $B1$ longitudinal side, captured from a direction tangential to the burner surface above the slit holes as shown in (a). Operation at 4 kW with an hydrogen content $P_{H_2} = 50\%$ at equivalence ratios (b) 0.50, (c) 0.45 and (d) 0.40.

First, the effect of H_2 substitution is considered and, secondly, the impact of the ports distribution is discussed. Figures 7(b-d) and 8(b-d) correspond to specific operating conditions presented in Fig. 6(a) for burner $B1$. The windows of investigation are illustrated in Figs. 7(a) and 8(a), while

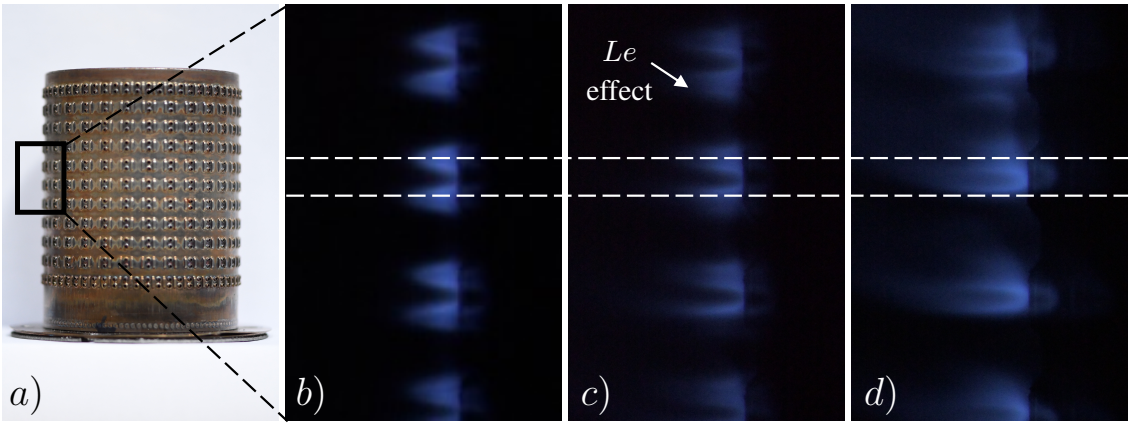

Figure 9: Flame shape along burner $B2$ longitudinal side, captured from a direction tangential to the burner surface above round holes as shown in (a). Operation at 4 kW with an hydrogen content $P_{H_2} = 50\%$ at equivalence ratios (b) 0.60, (c) 0.55 and (d) 0.50.

the white-dotted lines represent the axis of two adjacent burner holes.

On one side, Figures 7(b-d) show pure-CH_4 flames for equivalence ratios $\phi_g = 0.70$, 0.65 and 0.55. In Fig. 7(b), flames are attached to the burner surface at $\phi_g = 0.70$ and a series of independent conical reaction fronts develop beyond each slit hole. Reducing ϕ_g results in a simultaneous increase of the bulk flow velocity U_b and a reduction of the adiabatic laminar burning velocity S_L, which concomitantly lead to a gradual increase in the flame length and a coalescence of adjacent conical flame fronts as shown in Fig. 7(c). This phenomenon is exacerbated in Fig. 7(d) where the entire reaction layer detaches from the burner surface, resulting in a severe blow-off.

On the other side, Figs. 8(b-d) show for the same burner $B1$ H_2-enriched flame images ($P_{H_2} = 50\%$) at $\phi_g = 0.50$, 0.45 and 0.40, respectively. Figure 8(b), similar to Fig. 7(b), illustrates well-anchored flames and stable combustion. However, a reduction of ϕ_g to 0.45 marks a strong difference with respect to pure methane case: the flames lengthen and their curvatures increase, leading to flame tip-opening as in Fig. 8(c). This effect is due to the low Le number of molecular H_2 [16, 41, 42], which alters the properties of the mixture leading to a preferential diffusion within the flame front. According to [43] and considering the Le number of CH_4 (H_2) equal to 1.0 (0.3), the characteristic Le number of the fuel blend at $P_{H_2} = 50\%$ drops to 0.46, justifying the observation of thermodiffusive effects [44, 45]. As a consequence, the flame tip is quenched while the reaction rate strengthens at

the base of the conical flames. For that reason the reaction front shifts towards the periphery of the burner outlets promoting interactions among adjacent flames. Fig. 8(d) shows that this trend is intensified at blow-off conditions, in which the reaction zones lie entirely between burner ports.

To sum up, Le effects due to hydrogen addition promotes a different flame stabilization at very lean conditions (i.e. during blow-off). In case of CH_4-air mixtures the flames detach from the burner surface as a continuous reactive layer. In case of hydrogen enrichment, instead, single flames stabilize in the low velocity region among the burner outlets, where combustion is sustained thanks to the interaction among several holes. This mechanism strengthens by increasing the hydrogen substitution and it is reasonable to expect that it also depends on the ports distribution over the burner surface. This is further discussed in Fig. 9(b-d), in which the burner $B2$ is considered. This figure shows the blow-off transition for $P_{\mathrm{H_2}} = 50\%$ and equivalence ratios $\phi_{\mathrm{g}} = 0.60$, 0.55, 0.50. Figure 9(b) shows M flames stabilized along the burner wall, where each lobe corresponds to a single outlet of the burner. In analogy with Fig. 8, when the equivalence ratio is reduced, Le effects make the reaction rate stronger at the flame base and weaker at the flame tip (Fig. 9(c)). A further reduction of the equivalence ratio to 0.50 (Fig. 9(d)) produces a stabilization of the flame fronts between the two holes that are close to each other, while the reaction is quenched elsewhere. On one side, this observation confirms that the molecular diffusivity of hydrogen addition might promote a change of flame stabilization that increases the blow off resistance. On the other side, Figs. 9(d) shows that this mechanism is promoted by the proximity of the the burner holes. For burner $B2$, in fact, the distance between burner holes varies and H_2-enriched flames stabilize only if two holes are sufficiently close to each other. In the vicinity of the holes, hydrogen diffuses laterally encountering a relatively high-temperature and low-velocity region that enables flame stabilization. Moreover, limiting the distance between holes inhibits dilution by external air engulfment, which normally acts at the base of isolated Bunsen flames favoring local quenching [46, 47].

This interpretation requires the local flow velocity between the holes to be comparable to the hydrogen diffusion velocity in air at these thermodynamic conditions. This is verified considering the burner $B1$. In this setup, the hydrogen diffusion velocity $V_{\mathrm{d,H_2}}$ into air can be evaluated using Fick's law, under the hypothesis of constant mass fraction gradient of H_2 over the distance $l = 2.5$ mm between the hole axis and the mid point between two consecutive holes (see Fig. 10(b)). If the mass fraction of H_2 is considered to be equal to the value of the incoming premixed gases at the burner hole axis and linearly decreases to zero at the mid point between two consecutive holes, then

$V_{\mathrm{d,H_2}}$ is of the order of 0.25 m/s. The flow velocity component U_r along the burner radial direction is measured in non-reactive conditions (see sec. 3.1), imposing a volumetric flow rate representative of reactive operating conditions at 4 kW. Figure 10 shows U_r with respect to the axial direction of the burner, taken at a distance $d = 0.5$ mm above the burner surface. Interestingly, despite the maximum velocity being around 3 m/s, U_r drops below 0.3 m/s between two adjacent holes, reaching similar values of the H_2 diffusion velocity $V_{\mathrm{d,H_2}}$ evaluated previously. Hence, the local flow velocity is comparable with the diffusion velocity of hydrogen in air and so compatible with the conjectured mechanism of preferential diffusion.

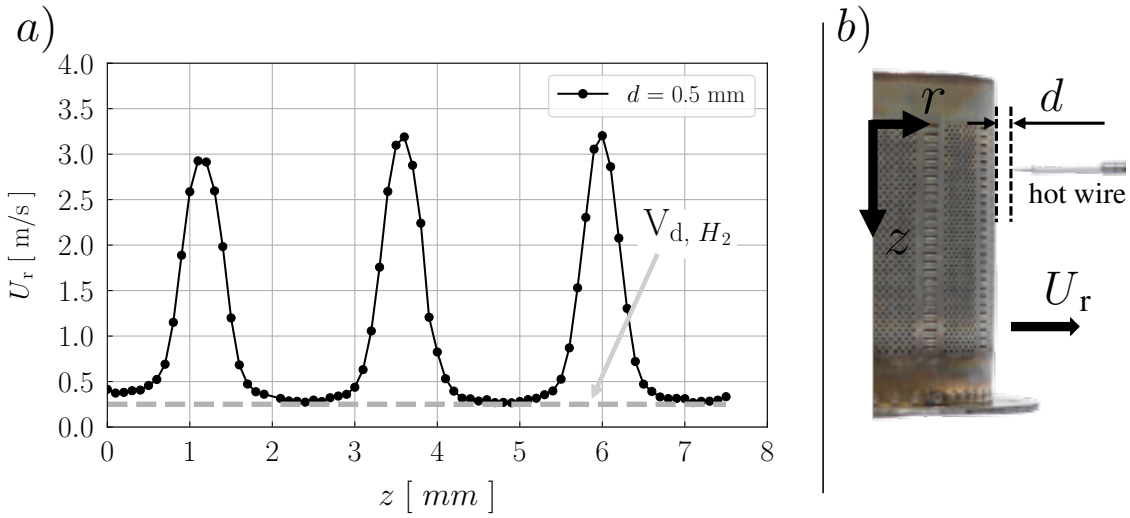

Figure 10: The radial velocity profile U_r, measured along the axial direction of burner $B1$ at $d = 0.5$ mm above the external surface (———), is compared to an estimation of the hydrogen diffusion velocity at the burner outlets (- - - -) (a). The axial and radial directions are indicated in (b), as well as the distance d at which the velocity profile is determined.

Overall, the discussion above suggests that either H_2-enrichment and a specific hole pattern must be considered to interpret flame stabilization, since both are necessary but not sufficient conditions to allow different flame stabilizations. These experiments also suggest that, in addition to the increased reactivity of H_2-enriched mixtures, a specific distribution of the burner holes can reinforce the blow-off resistance when H_2 is involved due to its high diffusion velocity.

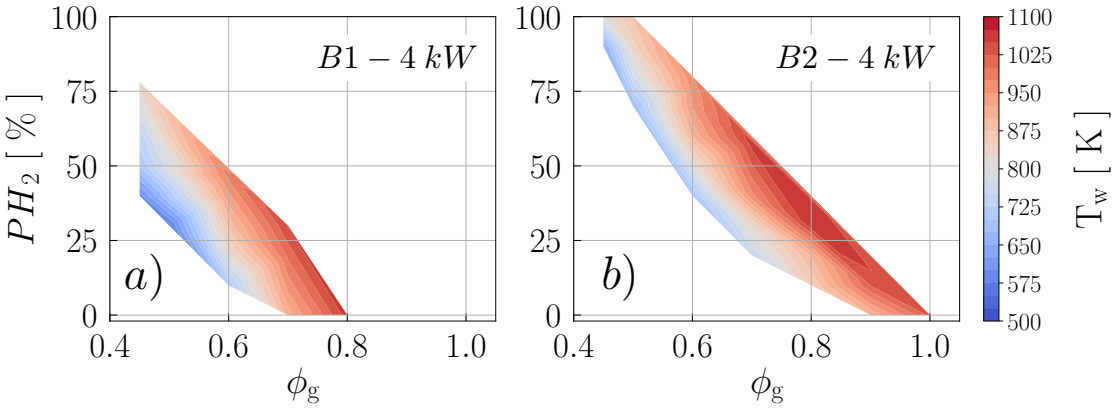

Figure 11: Wall temperature T_w contour maps as function of the hydrogen content P_{H_2} and equivalence ratio ϕ_g for burner $B1$ (a) and $B2$ (b) at power of 4 kW.

6. Effect of flame stabilization on the burner thermal load

The burner surface temperature T_w controls the lifetime of materials and it affects the mixture reactivity, since fresh gases are heated by the hot walls. The impact of the wall temperature T_w on flame stabilization is explored in this section. Figures 11(a-b) display the contour maps of surface temperature T_w at 4 kW for both burners. Data are retrieved by interpolating the temperature measurements collected with the pyrometer at steady state conditions over the operating points covered in Figs. 6(a-b). Here T_w represents the temperature at location 4 displayed in Fig. 5(a-b). The wall temperature T_w depends on the adiabatic flame temperature T_{ad} and on the stand-off distance η between the flame root and the flame holder. As demonstrated for example in case of flat flames [25, 26], these two parameters generally control the heat load on the burner. However, data listed in Tab. 4 demonstrate that T_{ad} does not correlate to T_w, at least for the conditions investigated. For instance, for operating conditions 3 and 5 T_w reaches comparable values but the corresponding adiabatic flame temperature T_{ad} differs by 130 K. An additional example is given considering operating conditions 1 and 5. In this case the adiabatic flame temperature is similar for both conditions, while T_w differs by more than 150 K. Interestingly, Table 4 shows that the wall temperature T_w results in a better correlation with the laminar burning velocity ${S_L}^{T_u}$, rather than with T_{ad}. In fact, as S_L increases with both equivalence ratio ϕ_g and fraction of hydrogen P_{H_2} in the fuel blend, the burner surface temperature T_w increases consistently. Here ${S_L}^{T_u}$ is retrieved

	ϕ_g - P_{H_2}	T_u (K)	$S_L{}^{T_a}$ (cm/s)	$S_L{}^{T_u}$ (cm/s)	T_w (K)	$T_{ad}{}^{T_u}$ (K)
1.	0.6 - 10%	407 ± 10	14.4	28.9	710 ± 2.1	1765
2.	0.6 - 20%	481 ± 12	17.8	54.1	813 ± 2.4	1838
3.	0.6 - 30%	512 ± 9	22.1	78.2	883 ± 2.6	1878
4.	0.6 - 40%	530 ± 8	26.8	105.0	943 ± 2.8	1909
5.	0.5 - 62%	521 ± 11	20.0	91.6	863 ± 2.6	1748

Table 4: Five operating conditions obtained with burner $B1$ at 4 kW are compared in terms of wall temperature T_w, adiabatic flame temperature T_{ad} and laminar burning velocity S_L, which is calculated considering fresh gases at T_a = 300 K and at T_u. The laminar burning velocity is highly affected by the fresh gas temperature T_u. T_w results in good correlation with $S_L^{T_u}$, rather than $T_{ad}^{T_u}$.

from CANTERA 1D simulations imposing T_u as unburnt gas temperature.

Flame stabilization is subjected to a positive feedback loop. An increase in T_w preheats the reactants at T_u resulting in larger $S_L^{T_u}$ and a flame closer to the wall, thus increasing T_w. Table 4 shows the impact of the fresh gas temperature T_u on the laminar burning velocity $S_L{}^{T_u}$ that is between 2 to 4 times higher than considering ambient conditions $S_L{}^{T_a}$. This also means that the mixture composition and the thermal state of the burner are strictly coupled, which needs to be taken into account in view of the fact that this interaction can affect flashback directly [46, 47, 48].

To highlight the actual variation of the stand-off distance η with increasing H_2 substitution, Figs. 12 and 13 illustrate the evolution of the flame front position at constant equivalence ratio for burners $B1$ and $B2$ at 4 kW. Figures 12(a) and 13(a) depict the windows of investigation of the burners (as in section 5). Figures 12(b-d) refer to burner $B1$ at 4 kW and $\phi_g = 0.6$, varying the hydrogen power content P_{H_2} from 0% to 46%. In case of pure methane flames, the reaction front is detached from the burner surface (Fig. 12(b)) because this operating condition is close to the blow-off limit (Fig. 6(a)). An increment of P_{H_2} to 25% results in shorter flames, confirming the H_2 stabilization effect against blow-off. In Fig. 12(d), the hydrogen power content P_{H_2} is augmented to 46% and the H_2-enhanced flame reactivity drives the flame closer to the burner surface. The conical laminar flames in Fig. 12(c) transform into independent nearly flat flames anchored at the edges of the burner holes in Fig. 12(d) and the heat load on the burner reaches its maximum. Similar observations are made in Figs. 13(b-d) with the burner $B2$, when it is fueled with a growing hydrogen content at ϕ_g

= 0.7. The flame shapes differ with respect to those shown for burner $B1$ because of the distribution of the exit holes. Flames of burner $B2$ exhibit a "M" shape, where each lobe forms in the wake of a single burner hole. Boosting the hydrogen content P_{H_2} from 20% to 55%, the flames shorten continuously and the burner surface temperature T_w raises from 750 K to 1020 K. In both burners the reaction front approaches dangerously the burner hole outlets when the hydrogen content is increased (Figs. 12(d) and 13(d)). An exacerbation of this phenomenon leads to flashback.

7. Flashback limit description

Flashback occurs in premixed burners when the flame propagates upstream through the injection system [38], which can be the result of different mechanisms. The simplest criterion to interpret flashback is based on premixed flame kinematics. Since a premixed flame lies where the component of the flow velocity perpendicular to the flame front matches the local flame speed, flashback is expected when the laminar burning velocity S_L overcomes the incoming bulk flow velocity U_b. This can be seen as a particular case of the general theory of the velocity gradient [9, 10]. According to that and considering a laminar flow with a given velocity profile, flashback occurs when the flow velocity gradient at the wall equals the ratio between the laminar flame speed and the flame thickness. However, if a flame stabilizes above small holes or narrow tubes, this theory tends to lose its validity. In this case, heat losses increase lowering the flame reactivity and ultimately hindering its passage towards the injection system. In these conditions, the main governing parameters become the wall temperature T_w and the flame holder diameter [46, 47, 49]. Because of the high temperature reached by the burner walls and the substantial preheating of the fresh mixture, autoignition close to the hot metallic burner surfaces inside the burner should also be taken into consideration. In fact, depending on the mixture composition and flow field at the exit holes, the burner wall temperature may potentially serve as source of energy to ignite the mixture [50], triggering flashback.

Considering now the present study, Figs. 6(a-d) show three isolines representative of $U_b/S_l = 1$ calculated for three different gas temperatures T_u=300 K (red), 500 K (green) and 700 K (blue). While the slope of the isolines is in good agreement with the one of the experimental flashback limits, the measured gas temperature T_u for the points that belong to the flashback lines (Figs. 6(a-d)) is not constant and the ratio between the bulk flow velocity through a burner hole U_b and the laminar burning velocity S_L varies substantially as indicated in Tab. 5. This table lists five operating points for burner $B1$ at 4 kW, where two stable operating points are

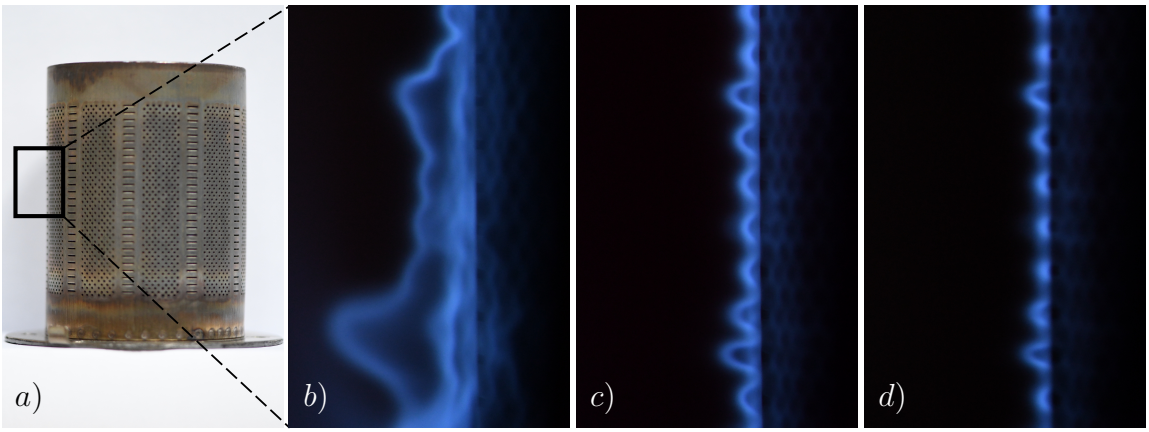

Figure 12: Flame shape evolution along burner $B1$ longitudinal side, captured from a direction tangential to the burner surface (a). Images correspond to steady state conditions for $\phi_g = 0.6$ and P_{H_2} equals to 0% (b), 25% (c) and 46% (d).

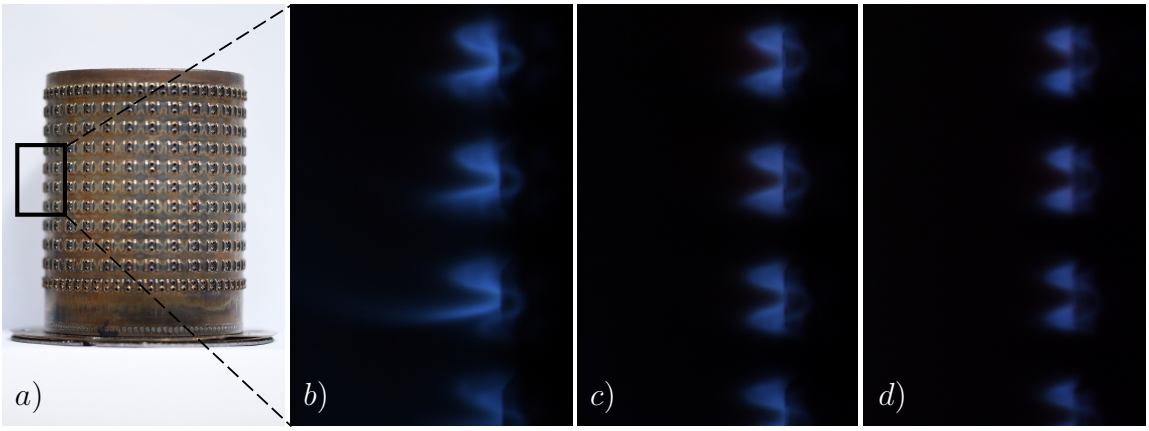

Figure 13: Flame shape evolution along burner $B2$ longitudinal side, captured from a direction tangential to the burner surface (a). Images correspond to steady state conditions for $\phi_g = 0.7$ and P_{H_2} equals to 20% (b), 40% (c) and 55% (d).

Description	ϕ_g ; P_{H_2}	T_u (K)	T_w (K)	$(U_b/S_L)_{T_u}$
Stable*	1.0 ; 0%	771 ± 4	1100 ± 3.3	1.1
Stable	0.8 ; 0%	692 ± 6	1060 ± 3.2	1.9
Flashback	0.6 ; 45%	594 ± 5	973 ± 2.9	1.8
Flashback	0.5 ; 62%	521 ± 11	863 ± 2.6	2.8
Flashback	0.45 ; 76%	499 ± 11	820 ± 2.5	3.3

Table 5: List of operating conditions used to investigate the role of the ratio between the bulk flow velocity U_b and the laminar burning velocity S_L with respect to flashback occurrence. This ratio is calculated for the gas temperature T_u(after being heated by the combustor walls), showing the decisive role of the unburned mixture temperature. The first stable condition identified by * is not included in the stabilization maps since the wall temperature T_w overcomes the overheating threshold of 1500 K, but is specifically considered in this table because of the low value of the ratio $(U_b/S_L)_{T_u}$.

compared to three conditions representative of flashback events. The ratio U_b/S_L is calculated considering flow and laminar burning velocity at the measured gas temperature T_u, showing that $(U_b/S_L)_{T_u}$ increases considerably with the hydrogen content P_{H_2} at different flashback conditions. Hence, the H_2-induced flashback cannot be simply predicted in view of the competition between the bulk velocity U_b and the laminar burning velocity S_L. With the goal of broadening the number of operating conditions subjected to flashback and investigate this phenomenon, a different measurement procedure is adopted. At the beginning, the burner is in thermal equilibrium with ambient. Then, the targeted mixture composition is imposed. After few seconds, the burner is ignited and the evolution of wall temperature with time is monitored. Three distinct regimes are identified after ignition:

Regime I: Combustion remains stable and the burner evolves naturally towards thermal equilibrium.

Regime II: Initially the flame stabilizes on the multi-perforated burner surface but, as T_w reaches a certain threshold, flashback occurs. This value is defined as $T_{w,fb}$.

Regime III: Ignition itself generates a sudden flashback. In this circumstance the flame is never stabilized on the burner, which remains at ambient temperature.

The maps presented in Figs. 14a-b show the regions of influence of the three different regimes for both burners. Most of the mixture compositions investigated in these additional unsteady

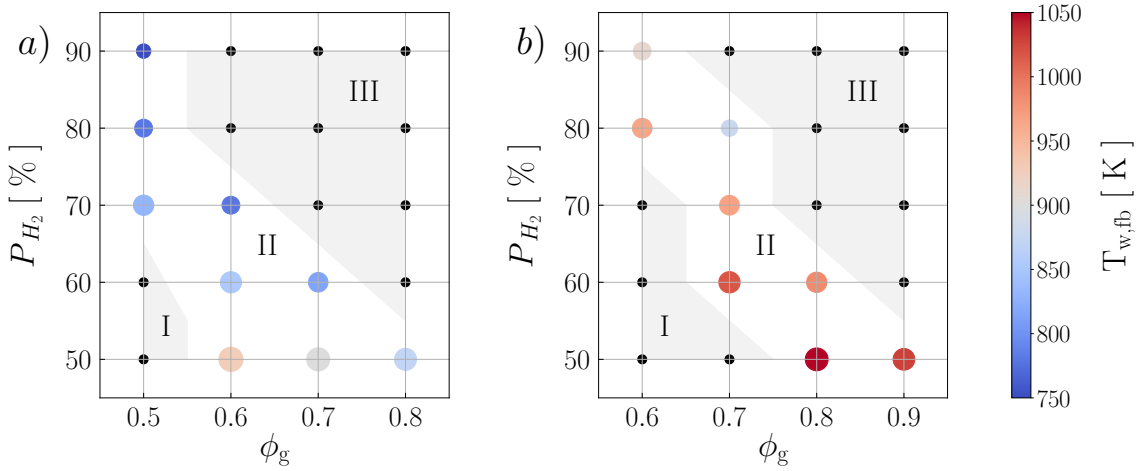

Figure 14: Description of the region of influence of regimes I, II and III with respect to the hydrogen power content P_{H_2} and equivalence ratio ϕ_g for burners $B1$ (a) and $B2$ (b). Operating conditions belonging to regime II are sized and colored considering the value of $T_{w,fb}$.

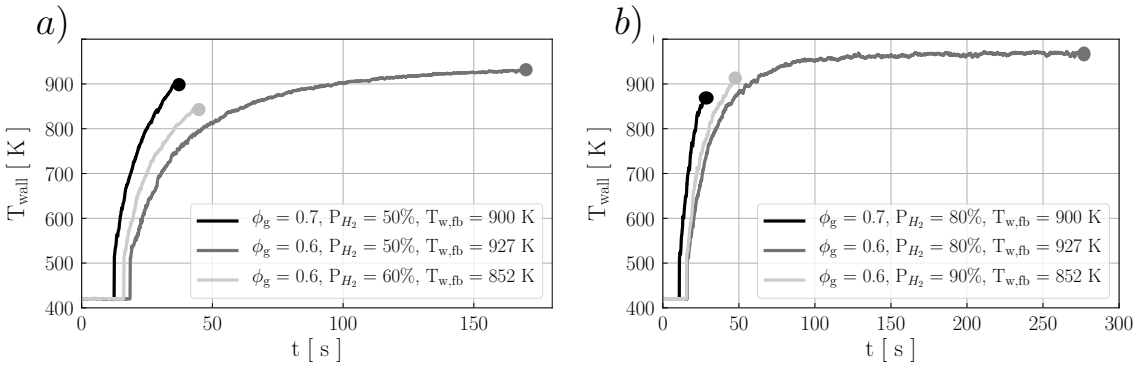

Figure 15: Burner surface temperature T_w time evolution from ignition to the instant at which flashback occurs is illustrated for three different mixtures and the two burners $B1$ (a) and $B2$ (b). Each curve shows the heating process of the burner till the condition $T_w = T_{w,fb}$ is attained.

experiments do not belong to the stabilization maps in Figs. 6a-b. In fact, it would be impossible to gather this level of insight operating the burner in quasi-steady state mode. As expected, only the operating conditions leading to regime I correspond to the ones displayed in Figs. 6a-b. At high equivalence ratio ϕ_{g} and large hydrogen power content $P_{\mathrm{H_2}}$, instead, the burners undergo flashback during ignition corresponding to regime III in Figs. 14a-b. For this pool of operating points, the reactivity of the mixture increases so much that it is impossible to operate the burners. In between these two regimes, there is a range of mixtures for which flashback is thermally activated by a specific burner surface temperature $T_{w,fb}$. This mechanism defines regime II. Both maps in Fig. 3 show that this limit can be attained from regime I either by increasing the hydrogen power content $P_{\mathrm{H_2}}$ or raising the equivalence ratio ϕ_{g} towards stoichiometry. Moreover, results reveal that this transition depends on the burner design.

Regime II identifies a strict dependence between flashback and the thermal state of the burner. Figures 15a-b display the evolution of the burner surface temperature T_w, after ignition, for three different mixture compositions with burners $B1$ and $B2$. In each case the wall temperature T_{w} increases up to a peculiar value $T_{w,fb}$ at which flashback occurs. It was verified that this value only depends on the mixture composition and it is not related to the time needed to attain $T_{w,fb}$. As shown, increasing either the hydrogen power content $P_{\mathrm{H_2}}$ or equivalence ratio ϕ_{g} leads to a reduction of this activation temperature, presumably due to the boosted reactivity of the mixture. Figure 15b, for instance, puts in evidence that increasing $P_{\mathrm{H_2}}$ from 80% to 90% at constant ϕ_{g} = 0.6, reduces $T_{w,fb}$ from 967 K to 912 K. On the other side, increasing ϕ_{g} to 0.7 keeping $P_{\mathrm{H_2}}$ constant to 80%, reduces $T_{w,fb}$ to 880 K. Measurements have been repeated at least three times for each condition and the variation of T_w^{fb} lies within $\pm$5 K, which is below the instrumentation error. Furthermore, Figs. 14a-b illustrate that burner $B1$ undergoes flashback for a wall temperature that is lower than for burner $B2$. This is particularly evident for a hydrogen power content $P_{\mathrm{H_2}}$ = 50% and equivalence ratio ϕ_{g} = 0.8, which is the unique point shared by the two burners lying in regime II. In this case, $T_{w,fb}$ is equal to 872 K for burner $B1$, while it increases to 1068 K for burner $B2$. Despite results highlight the crucial role of the wall temperature T_{w}, they do not shed lights on the fundamental mechanisms that drive this process and additional work is needed to interpret the observations made.

8. Conclusions

Hydrogen hybridization of two commercial premixed burners, used in condensing boiler applications and designed to operate with natural gas - air mixtures, has been investigated. The burners are tested in the low-power range, analyzing blow-off and flashback limits over a wide range of equivalence ratio for methane, hydrogen and air mixtures. Stability maps demonstrate that H_2 addition improves the blow-off resistance, but it also limits the maximum achievable equivalence ratio due to occurrence of overheating or flashback, leaving the range of stable operating conditions roughly unchanged. Because of these constraints, pure hydrogen combustion is possible only at ultra-lean conditions, while the maximum hydrogen concentration for a given thermal power and equivalence ratio is found to be variable with the burner design.

The study underlines the impact of hydrogen low Le number on lean flame stabilization. To this regard, it has been highlighted a specific mechanism that contributes to blow-off resistance related to hydrogen diffusion properties, through which flames stabilize in the near-surface region among holes rather than in their wake.

For a fixed equivalence ratio, the increment of H_2 enrichment above a certain threshold leads to flashback. It has been shown that this limit is strongly related to the burner wall temperature T_{w}. The three regimes have been identified depending on the mixture composition and on the burner design. The first regime (I) is characterized by stable flame stabilization, without risk of flashback. In regime II, flashback is piloted by the thermal state of the burner and occurs at a specific wall temperature $T_{\mathrm{w}} = T_{w,fb}$. This threshold temperature $T_{w,fb}$ decreases with increasing the reactivity of the mixture. In regime III, flashback occurs during the ignition process, irrespective of the burner wall temperature T_{w}. This regime is characterized by very high hydrogen content and equivalence ratio close to stoichiometry.

Further studies will be focused on this specific issue to shed lights on the fundamental mechanisms that drive flashback in this kind of systems with the objective of designing a concept burner suitable for full H_2 combustion over a wide range of equivalence ratio.

9. Acknowledgements

This project has received funding from the European Research Council under the European Union's Horizon 2020 research and innovation programme Grant Agreement 832248, SCIROCCO and under

the Horizon 2020, COEC (Center of Excellence in Combustion) program, Grant Agreement 952181.

References

[1] G. Gahleitner, Hydrogen from renewable electricity: An international review of power-to-gas pilot plants for stationary applications, International Journal of Hydrogen Energy 38 (5) (2013) 2039–2061. doi:https://doi.org/10.1016/j.ijhydene.2012.12.010.

[2] M. D. Cabezas, J. I. Franco, H. J. Fasoli, Optimization of self-regulated hydrogen production from photovoltaic energy, International Journal of Hydrogen Energy 45 (17) (2020) 10391–10397, aEM 2018 - Smart Materials for Hydrogen Energy. doi:https://doi.org/10.1016/j.ijhydene.2018.10.203.

[3] H. Levinsky, Why can't we just burn hydrogen? challenges when changing fuels in an existing infrastructure, Progress in Energy and Combustion Science 84 (2021) 100907. doi:https://doi.org/10.1016/j.pecs.2021.100907.

[4] F. Schiro, A. Stoppato, A. Benato, Modelling and analyzing the impact of hydrogen enriched natural gas on domestic gas boilers in a decarbonization perspective, Carbon Resources Conversion 3 (2020) 122–129. doi:https://doi.org/10.1016/j.crcon.2020.08.001.

[5] A. L. Sánchez, F. A. Williams, Recent advances in understanding of flammability characteristics of hydrogen, Progress in Energy and Combustion Science 41 (2014) 1–55. doi:https://doi.org/10.1016/j.pecs.2013.10.002.

[6] Y. Zhao, V. McDonell, S. Samuelsen, Influence of hydrogen addition to pipeline natural gas on the combustion performance of a cooktop burner, International Journal of Hydrogen Energy 44 (23) (2019) 12239 – 12253. doi:https://doi.org/10.1016/j.ijhydene.2019.03.100.

[7] Y. Zhao, V. McDonell, S. Samuelsen, Experimental assessment of the combustion performance of an oven burner operated on pipeline natural gas mixed with hydrogen, International Journal of Hydrogen Energy 44 (47) (2019) 26049 – 26062. doi:https://doi.org/10.1016/j.ijhydene.2019.08.011.

[8] S. Choudhury, V. G. McDonell, S. Samuelsen, Combustion performance of low-nox and conventional storage water heaters operated on hydrogen enriched natural gas, International

Journal of Hydrogen Energy 45 (3) (2020) 2405 – 2417. doi:https://doi.org/10.1016/j.ijhydene.2019.11.043.

[9] G. von Elbe, M. Mentser, Further studies of the structure and stability of burner flames, The Journal of Chemical Physics 13 (2) (1945) 89–100. doi:10.1063/1.1724004.

[10] B. Lewis, G. von Elbe, Stability and structure of burner flames, The Journal of Chemical Physics 11 (2) (1943) 75–97. doi:10.1063/1.1723808.

[11] R. M. M. Mallens, H. C. de Lange, C. H. J. van de Ven, L. P. H. de Goey, Modeling of confined and unconfined laminar premixed flames on slit and tube burners, Combustion Science and Technology 107 (4-6) (1995) 387–401. doi:10.1080/00102209508907812.

[12] S. Plee, A. Mellor, Review of flashback reported in prevaporizing/premixing combustors, Combustion and Flame 32 (1978) 193 – 203. doi:https://doi.org/10.1016/0010-2180(78)90093-7.

[13] S. Lee, J. T'ien, A numerical analysis of flame flashback in a premixed laminar system, Combustion and Flame 48 (1982) 273–285. doi:10.1016/0010-2180(82)90134-1.

[14] T. Echekki, M. Mungal, Flame speed measurements at the tip of a slot burner: Effects of flame curvature and hydrodynamic stretch, Symposium (International) on Combustion 23 (1) (1991) 455–461. doi:https://doi.org/10.1016/S0082-0784(06)80291-2.

[15] G. I. Sivashinsky, Structure of bunsen flames, The Journal of Chemical Physics 62 (2) (1975) 638–643. doi:10.1063/1.430465.

[16] T. M. Vu, M. S. Cha, B. J. Lee, S. H. Chung, Tip opening of premixed bunsen flames: Extinction with negative stretch and local karlovitz number, Combustion and Flame 162 (4) (2015) 1614–1621. doi:https://doi.org/10.1016/j.combustflame.2014.11.022.

[17] B. C. Duva, E. Toulson, Unstretched unburned flame speed and burned gas markstein length of diluted hydrogen/air mixtures, International Journal of Hydrogen Energy (2022). doi:https://doi.org/10.1016/j.ijhydene.2021.12.217.

[18] A. Ern, V. Giovangigli, Thermal diffusion effects in hydrogen-air and methane-air flames, Combustion Theory and Modelling 2 (4) (1998) 349–372. doi:10.1088/1364-7830/2/4/001.

[19] P. Pelce, P. Clavin, Influence of hydrodynamics and diffusion upon the stability limits of laminar premixed flames, Journal of Fluid Mechanics 124 (1982) 219–237. doi:10.1017/S002211208200247X.

[20] H. Altay, S. Park, D. Wu, D. Wee, A. Annaswamy, A. Ghoniem, Modeling the dynamic response of a laminar perforated-plate stabilized flame, Proceedings of the Combustion Institute 32 (1) (2009) 1359–1366. doi:10.1016/j.proci.2008.06.099.

[21] L. de Goey, J. van Oijen, V. Kornilov, J. ten Thije Boonkkamp, Propagation, dynamics and control of laminar premixed flames, Proceedings of the Combustion Institute 33 (1) (2011) 863–886. doi:10.1016/j.proci.2010.09.006.

[22] D. Mejia, L. Selle, R. Bazile, T. Poinsot, Wall-temperature effects on flame response to acoustic oscillations, Proceedings of the Combustion Institute vol. 35 (n° 3) (2015) 3201–3208. doi:10.1016/j.proci.2014.07.015.
URL https://hal.archives-ouvertes.fr/hal-01116177

[23] H. M. Altay, K. S. Kedia, R. L. Speth, A. F. Ghoniem, Two-dimensional simulations of steady perforated-plate stabilized premixed flames, Combustion Theory and Modelling 14 (1) (2010) 125–154. doi:10.1080/13647831003660859.

[24] K. S. Kedia, A. F. Ghoniem, Mechanisms of stabilization and blowoff of a premixed flame downstream of a heat-conducting perforated plate, Combustion and Flame 159 (3) (2012) 1055 – 1069. doi:https://doi.org/10.1016/j.combustflame.2011.10.014.

[25] C. R. Ferguson, J. C. Keck, Stand-off distances on a flat flame burner, Combustion and Flame 34 (1979) 85 – 98. doi:https://doi.org/10.1016/0010-2180(79)90080-4.

[26] L. P. H. de Goey, A. van Maaren, R. M. Quax, Stabilization of adiabatic premixed laminar flames on a flat flame burner, Combustion Science and Technology (1993). doi:10.1080/00102209308907668.

[27] Y. Ding, D. Durox, N. Darabiha, T. Schuller, Chemiluminescence of burner-stabilized premixed laminar flames, Combustion Science and Technology 191 (1) (2019) 1–25. doi:10.1080/00102202.2018.1558391.

[28] H. Dai, B. Zhang, Z. Li, J. Wu, Combustion characteristics of a porous media burner with partial hydrogen injection, International Journal of Hydrogen Energy 47 (2) (2022) 1092–1102. doi:https://doi.org/10.1016/j.ijhydene.2021.10.042.

[29] S. Lee, S. M. Kum, C. E. Lee, An experimental study of a cylindrical multi-hole premixed burner for the development of a condensing gas boiler, Energy 36 (7) (2011) 4150–4157. doi:10.1016/j.energy.2011.04.029.

[30] J. E. Veetil, C. Rajith, R. K. Velamati, Numerical simulations of steady perforated-plate stabilized syngas air pre-mixed flames, International Journal of Hydrogen Energy 41 (31) (2016) 13747–13757. doi:10.1016/j.ijhydene.2016.06.120.

[31] S. Lee, S. M. Kum, C. E. Lee, Performances of a heat exchanger and pilot boiler for the development of a condensing gas boiler, Energy (2011). doi:10.1016/j.energy.2011.05.018.

[32] J. Hinrichs, D. Felsmann, S. S.-D. Bortoli, H.-J. Tomczak, H. Pitsch, Numerical and experimental investigation of pollutant formation and emissions in a full-scale cylindrical heating unit of a condensing gas boiler, Applied Energy 229 (2018) 977–989. doi:10.1016/j.apenergy.2018.08.011.

[33] F. Schiro, A. Stoppato, Experimental investigation of emissions and flame stability for steel and metal fiber cylindrical premixed burners, Combustion Science and Technology (2018). doi:10.1080/00102202.2018.1500556.

[34] A. González-Espinosa, A. Gil, L. Royo-Pascual, A. Nueno, C. Herce, Effects of hydrogen and primary air in a commercial partially-premixed atmospheric gas burner by means of optical and supervised machine learning techniques, International Journal of Hydrogen Energy 45 (55) (2020) 31130–31150. doi:https://doi.org/10.1016/j.ijhydene.2020.08.045.

[35] F. Schiro, A. Stoppato, A. Benato, Potentialities of hydrogen enriched natural gas for residential heating decarbonization and impact analysis on premixed boilers, E3S Web Conf. 116 (2019) 00072. doi:10.1051/e3sconf/201911600072.

[36] F. Schiro, A. Stoppato, A. Benato, Gas fired boilers: Perspective for near future fuel composition and impact on burner design process, E3S Web Conf. 22 (2017) 00154. doi:10.1051/e3sconf/20172200154.

[37] M. K. Büyükakın, S. Öztuna, Numerical investigation on hydrogen-enriched methane combustion in a domestic back-pressure boiler and non-premixed burner system from flame structure and pollutants aspect, International Journal of Hydrogen Energy 45 (60) (2020) 35246–35256. doi:https://doi.org/10.1016/j.ijhydene.2020.03.117.

[38] A. Kalantari, V. McDonell, Boundary layer flashback of non-swirling premixed flames: Mechanisms, fundamental research, and recent advances, Progress in Energy and Combustion Science 61 (2017) 249–292. doi:https://doi.org/10.1016/j.pecs.2017.03.001.

[39] R. Schefer, D. Wicksall, A. Agrawal, Combustion of hydrogen-enriched methane in a lean premixed swirl-stabilized burner, Proceedings of the Combustion Institute 29 (1) (2002) 843–851, proceedings of the Combustion Institute. doi:https://doi.org/10.1016/S1540-7489(02)80108-0.

[40] A. F. Ghoniem, A. Annaswamy, S. Park, Z. C. Sobhani, Stability and emissions control using air injection and h2 addition in premixed combustion, Proceedings of the Combustion Institute 30 (2) (2005) 1765–1773. doi:https://doi.org/10.1016/j.proci.2004.08.175.

[41] M. Mizomoto, Y. Asaka, S. Ikai, C. Law, Effects of preferential diffusion on the burning intensity of curved flames, Symposium (International) on Combustion 20 (1) (1985) 1933–1939. doi:https://doi.org/10.1016/S0082-0784(85)80692-5.

[42] Y. Mizobuchi, T. Nambu, T. Takeno, Numerical study of tip opening of hydrogen/air bunsen flame, Proceedings of the Combustion Institute 37 (2) (2019) 1775–1781. doi:https://doi.org/10.1016/j.proci.2018.05.025.

[43] N. Bouvet, F. Halter, C. Chauveau, Y. Yoon, On the effective Lewis number formulations for lean hydrogen/hydrocarbon/air mixtures, International Journal of Hydrogen Energy 38 (14) (2013) 5949–5960. doi:10.1016/j.ijhydene.2013.02.098.

[44] T. Howarth, A. Aspden, An empirical characteristic scaling model for freely-propagating lean premixed hydrogen flames, Combustion and Flame 237 (2022) 111805. doi:https://doi.org/10.1016/j.combustflame.2021.111805.

[45] L. Berger, A. Attili, H. Pitsch, Intrinsic instabilities in premixed hydrogen flames: Parametric variation of pressure, equivalence ratio, and temperature. part 1 - dispersion relations in the

linear regime, Combustion and Flame 240 (2022) 111935. doi:https://doi.org/10.1016/j.combustflame.2021.111935.

[46] L. E. Bollinger, R. Edse, Effect of burner-tip temperature on flash back of turbulent hydrogen-oxygen flames, Industrial & Engineering Chemistry 48 (4) (1956) 802–807. arXiv:https://doi.org/10.1021/ie50556a040, doi:10.1021/ie50556a040.

[47] G. L. Dugger, Flame stability of preheated propane-air mixtures, Industrial & Engineering Chemistry 47 (1) (1955) 109–114. arXiv:https://doi.org/10.1021/ie50541a038, doi:10.1021/ie50541a038.

[48] L. Khitrin, P. Moin, D. Smirnov, V. Shevchuk, Peculiarities of laminar- and turbulent-flame flashbacks, Symposium (International) on Combustion 10 (1) (1965) 1285–1291. doi:https://doi.org/10.1016/S0082-0784(65)80263-6.

[49] Y. Jung, M. J. Lee, N. I. Kim, Direct prediction of laminar burning velocity and quenching distance of hydrogen-air flames using an annular stepwise diverging tube (asdt), Combustion and Flame 164 (2016) 397–399. doi:https://doi.org/10.1016/j.combustflame.2015.12.005.

[50] L. Boeck, J. Melguizo-Gavilanes, J. Shepherd, Hot surface ignition dynamics in premixed hydrogen–air near the lean flammability limit, Combustion and Flame 210 (2019) 467–478. doi:https://doi.org/10.1016/j.combustflame.2019.09.002.